Composites Communications 36 (2022) 101383

Contents lists available at ScienceDirect

Composites Communications

journal homepage: www.elsevier.com/locate/coco

A compliant robotic grip structure based on shape memory polymer composite

Yonglin Zhang [a], Tianzhen Liu [a], Xin Lan [b], Yanju Liu [a], Jinsong Leng [b], Liwu Liu [a,*]

[a] Department of Astronautical Science and Mechanics, Harbin Institute of Technology (HIT), P.O. Box 301, No. 92 West Dazhi Street, Harbin, 150001, PR China
[b] Center for Composite Materials and Structures, Harbin Institute of Technology (HIT), P.O. Box 3011, No. 2 YiKuang Street, Harbin, 150080, PR China

ARTICLE INFO

Keywords:
Shape memory polymer composite
Compliant grip structure
Shape memory effect
Viscoelasticity

ABSTRACT

Functional structures based on shape memory polymer composites (SMPCs) are featured with the superiority of circumstance sensitivity, lightweight, and high loading capability. This work presents the design, fabrication, evaluation, and application of a compliant robotic grip structure based on SMPC. The grip structure was designed and fabricated with a configuration of curving SMPC finger for target capture function. Then, the material property of the SMPC sample was investigated by dynamic mechanical analysis (DMA), and the shape memory effect was modeled via the viscoelasticity described by the Prony series and WLF equation. The performance of the gripper was constructed and analyzed by finite element analysis (FEA), and experimental data verified the simulation results showing good agreement. Furthermore, the recovery force and recovery angle of a single SMPC gripper were estimated, and the results indicated a 100% deformation recovery and a maximum recovery force of 2.6 N. Finally, the functionality and adaptability of the system were illustrated and validated by workflow demonstration and various target tasks. This paper outlines the actuation mechanism, evaluation methods, and performance estimation of the proposed compliant robotic grip structure and shows the potential for promising industrial applications.

1. Introduction

Traditional actuation systems consist of components made of hard materials, mainly metals, but the requirements nowadays for the compliance capture of various targets exceed the capability of conventional methods. Therefore, soft robotic devices recently become an interest in academic and industrial research [1–3]. As the key components of soft actuation devices, the servo unit and execute unit are the heart and hand of the system, respectively. The actuation modes of servo units include the active pressure-driven technique [4,5], the passive contact-driven deformation technique [6,7], and the smart materials [8–10].

For the pressure-driven method and contact-driven method, the system requires external units to provide energy conservation, while smart materials show superiority in integration and convenience by offering actuation and operation within a single segment which is more straightforward and cost-saving. Typical smart materials for soft grip systems include dielectric elastomer polymers, shape-memory materials, etc. The actuators based on dielectric elastomer polymers can generate a large actuation strain range (over 1000%) [11] and rapid response speed (less than 0.2 ms) [12]. The configuration of self-organized dielectric elastomer minimum energy structures is developed and reported for grasping. The design and work principles were illustrated by Kofod et al. and the bending mode of the actuators was assigned to be the motion approach [13]. Representative shape memory materials include shape memory alloys (SMAs) and shape memory polymers (SMPs), and they return from a temporary deformed configuration to the initial shape by external stimulus [14,15]. SMAs exhibit the shape memory effect by the crystallographic transition between the martensite and austenite phases in response to temperature change. SMAs present high response stress (~hundreds of MPa) with significant elastic strain up to 5%, high elastic modulus (~100 GPa below transition temperature and ~10 GPa above transition temperature), minimization capability, and high thermal conductivity [16–18]. But the SMAs actuator's response presents magnificent hysteresis behavior, and requires for high power inputs [19,20]. SMPs react to an outside stimulus resulting by changing the transition domain phase of polymer networks from crystallization to melting, causing macro-scale deformation, and current stimulus variables include changes of heat, light, magnetism, electricity, humidity, and pH value. The low density of unreinforced or reinforced SMPs

* Corresponding author.
E-mail address: liuliwu_006@163.com (L. Liu).

https://doi.org/10.1016/j.coco.2022.101383
Received 26 July 2022; Received in revised form 15 October 2022; Accepted 17 October 2022
Available online 19 October 2022
2452-2139/© 2022 Published by Elsevier Ltd.

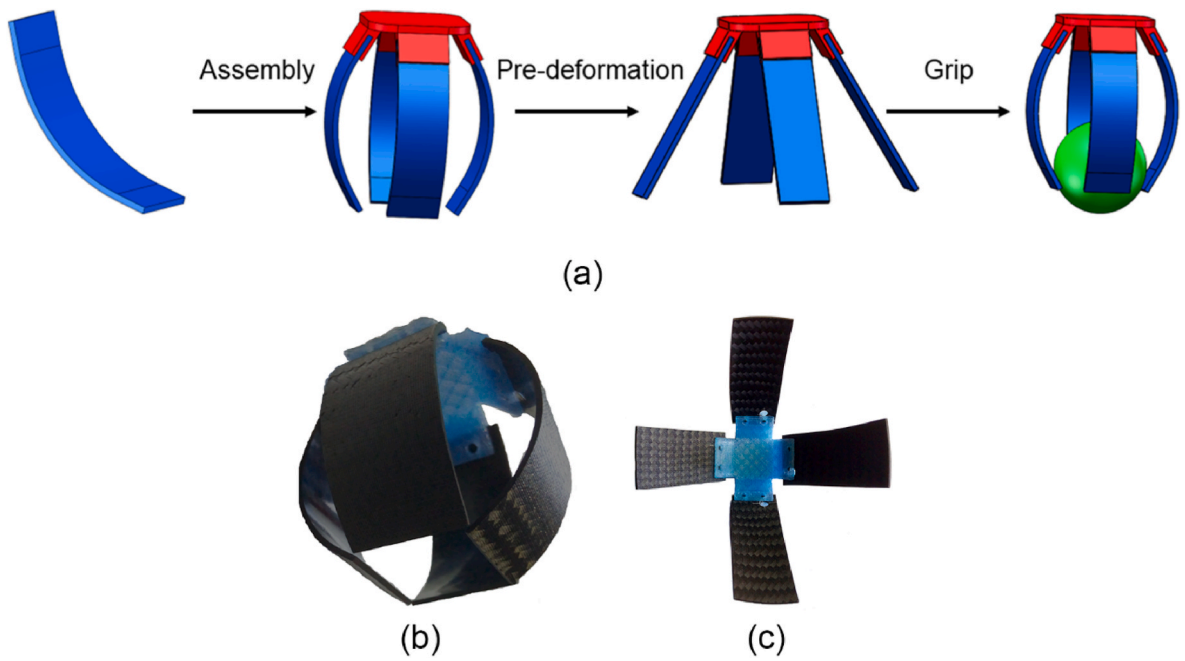

Fig. 1. The compliant robotic grip structure (a) Work process; (b) As assembled; (c) Deformed.

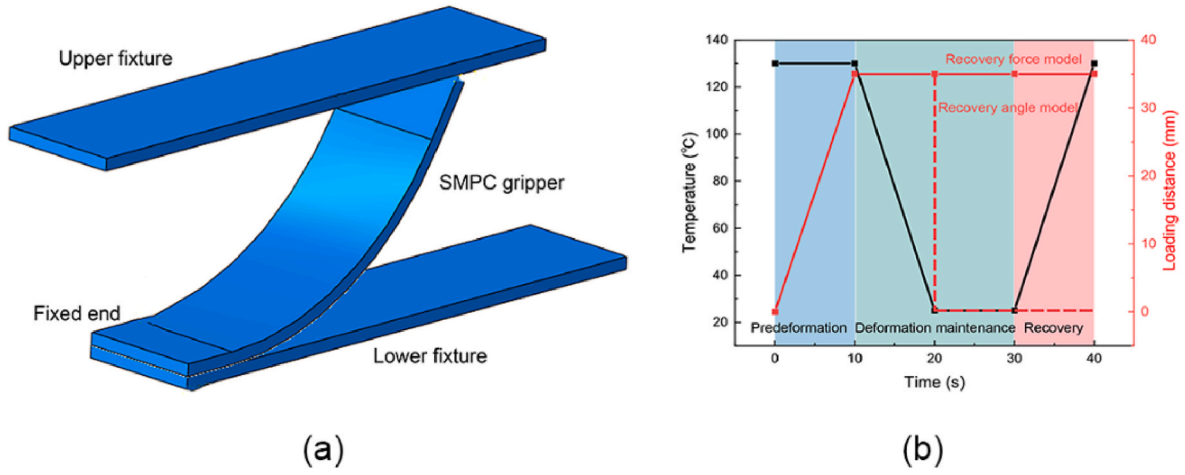

Fig. 2. Finite element model (a)Geometry and boundary condition; (b)Loading profile.

allows for the broad application in lightweight structures. The controllable activation temperature is another benefit that can be manipulated by changing the co-polymer composite or the cross-linking degree [21–23]. Shape-memory polymers composite is a multiphase composite using SMPs as a matrix by adding reinforcements like carbon fiber, carbon nanotube, nano-scale inorganic, organic substances and etc. [21,22]. SMPs have been assembled with other soft actuators to present variable stiffness components [24,25].

Comparing with SMPs, the carbon fiber reinforced shape memory polymer composites (SMPCs) have a higher elastic modulus as well as higher recovery force which is adequate for specific capture and loading tasks requiring high strength and reliability [26–28]. Currently, research is carried out mainly on concept construction, function demonstration, and phenomenological description, lacking insight into the mechanical behavior and subsequent system design guideline. In this work, we proposed a SMPC-based compliant robotic grip structure associated with a decision-making support methodology from a perspective of material property to structure evaluation to system performance for the development of the soft grip techniques.

2. Material and methodology

2.1. Material fabrication and structure assembly

The SMPC compliant robotic grip structure works following the process below as shown in Fig. 1(a). Firstly, a curving SMPC board was made of shape memory polymer resin and carbon fiber and then cut into curving beams. Four curving SMPC beams were installed on a plate to construct the grip structure. External force and tools deformed the curve SMPC grippers to straight beams under elevated temperature, and the deformed shape was obtained after cooling. In the grasp work process, the grip structure captured a target under heat stimulation as the straight beams recover.

We designed the compliant grip structure assembled with four SMPC grippers achieving soft grasp. The individual SMPC gripper part was designed as a curvature beam with the thickness of 2 mm, the width of 10 mm, the radius of 50 mm, and the radian of 60°. The curving SMPC was fabricated based on a thermoset SMP epoxy system via the vacuum-assisted resin transfer molding (VARTM) process as shown in Fig. 1(b),

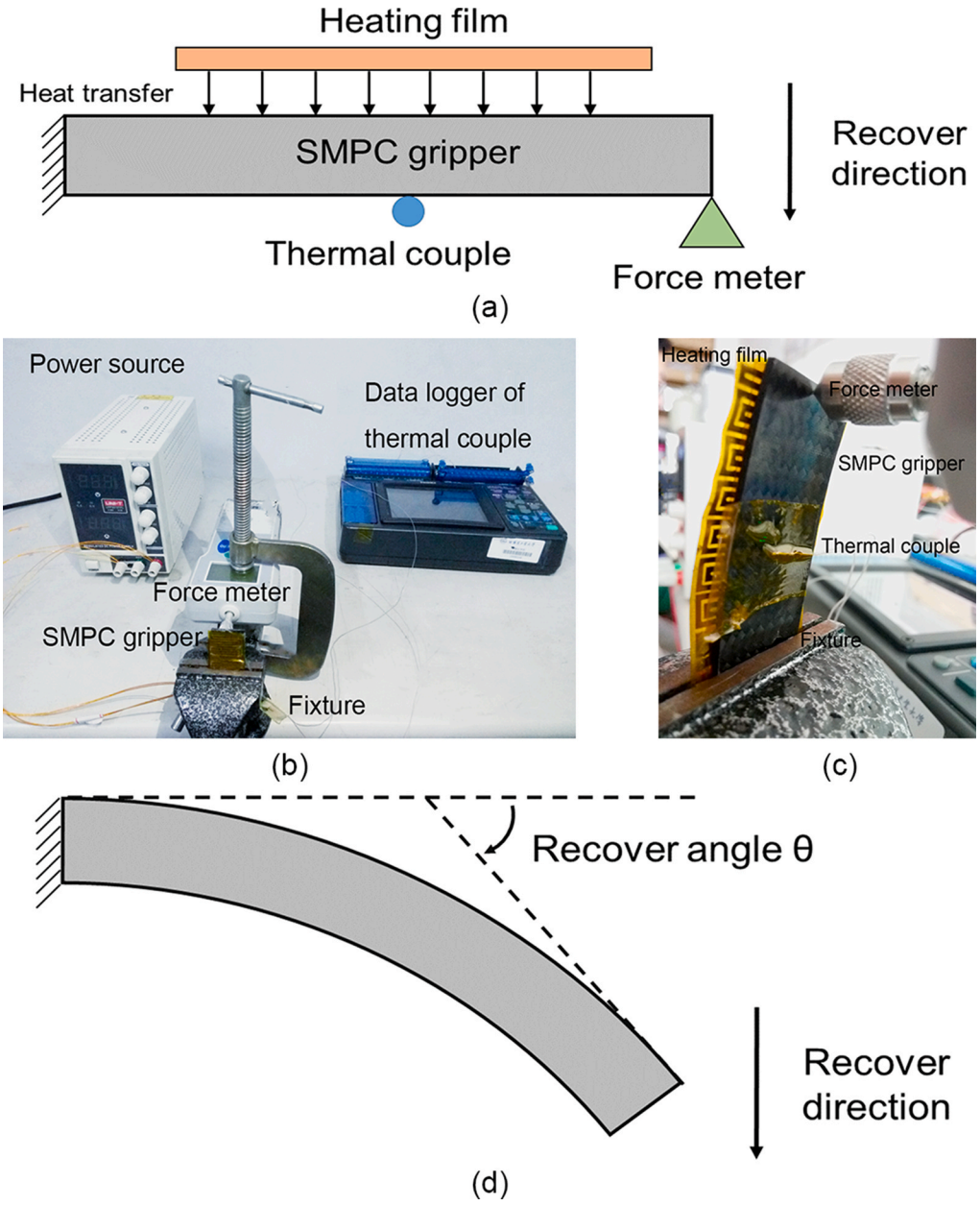

Fig. 3. Schematic of test system setup (a) Recovery force test; (b) Test system and test vehicle of recovery test; (c) SMPC gripper and facilities installation; (d) Recovery angle test.

Table 1
Prony series parameters.

i	τ_i (s)	E_i (MPa)
1	1e-3	69
2	1e-1	51
3	1e0	813
4	1e3	29
5	1e5	18
		$E_\infty = 210$

Table 2
WLF equation parameters.

Tr (°C)	C1	C2
130	17.44	85

(c). Due to the low density of resin and carbon fiber, the mass of each SMPC grip finger was 2.25g, and the whole structure weighed 15g which was incredible lighter compared to other rigid actuators. For the composition, the epoxy-based resin with shape memory effect was developed by Jinsong Leng's group [29], and the carbon fiber used was T300-3K type. Meanwhile, the weight fraction of resin and fiber are 84% and 16%, respectively.

2.2. Material property characterization

Dynamic mechanical analysis (DMA) was performed on the SMPC sample to obtain the thermomechanical property. In the test, the 3-point bending mode was employed, and span length, oscillation amplitude, heating rate, and loading frequency were 20 mm, 1 μm, 3 °C/min, and 1–100Hz, respectively.

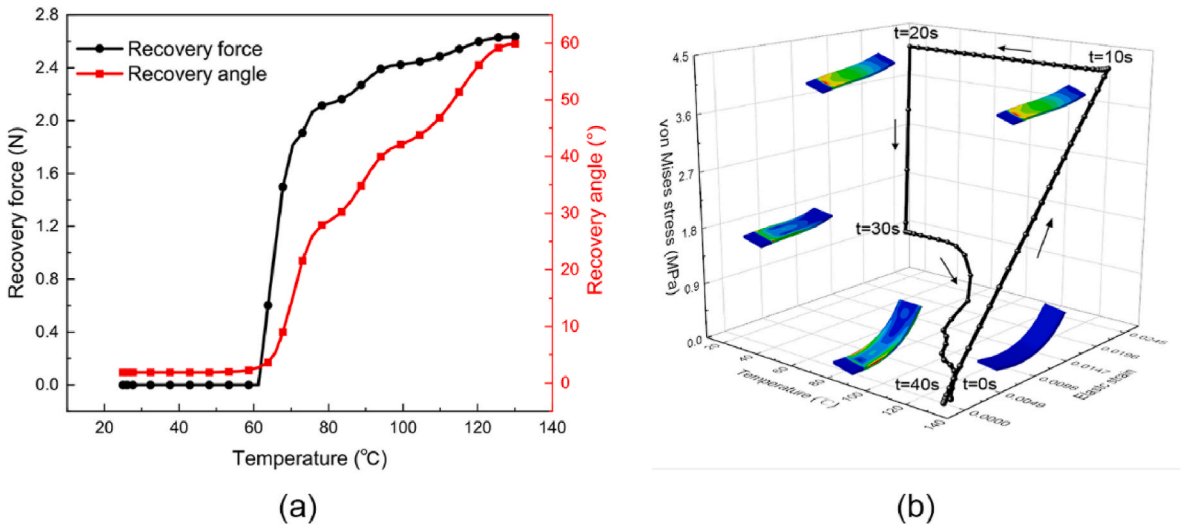

Fig. 4. Simulation results (a) Recovery force and angle; (b) Path of mechanical response during the shape memory cycle.

2.3. Finite element model

Finite element models were developed to investigate the shape memory behavior during the recovery force test and recovery angle test. As shown in Fig. 2(a), an individual SMPC gripper part was built with the left end fixed, and two plate fixtures were considered for predeformation, of which the lower one was completely fixed and the upper one was assigned to move downwards to press on the SMPC part. The loading profile, including the temperature and the upper fixture loading distance is shown in Fig. 2(b). Initially, in the predeformation phase, the temperature was set as 130 °C, and the loading distance for the upper fixture increased linearly to 35 mm in 10s. In the deformation maintenance phase, the temperature was gradually reduced to 25 °C in 10s and maintained for 10s, and the loading distance was held in the recovery force model as the solid red line, while the fixture removes in the recovery angle model as the dash red line. In the recovery phase, the SMPC part was heated to 130 °C, and the fixtures stayed unmoved during this period.

The material property obtained from the DMA data was assigned for the SMPC part, and the fixtures were set as rigid bodies. Since the data obtained from the DMA test was conducted with a 3-point mode which was consistent with the deformation pattern in the work process, hereby the data was appropriate for the material property assignment for the simulation. The temperature distribution was assumed to be uniform inside the part. In the model, we neglected the entity of the heating film with reasonable consideration and simplification. The mechanical effect of the film was removed due to the insignificant contribution of the thin PI film and copper coil, and the thermal effect was built by the temperature assignment. For the meshing, 23840 linear hexahedral elements of type C3D8R and 30750 nodes were created. Visco analysis steps were assigned for the creep behavior simulation.

2.4. Evaluation of shape memory effect

The experimental work on the shape memory effect was carried out in two separate tests, the recovery force test, and the recovery angle test. The experimental system setup is depicted in Fig. 3. As shown in Fig. 3 (a) and (b), in the recovery force test, one end of a deformed single SMPC gripper was fixed, and another end was fixed against on a force meter. A heating film was pasted on the top surface of the SMPC grip finger as a heating source, and a thermal couple associated with Hioki MEMORY HiLOGGER LR8400 portable data logger was attached to the other surface to monitor the temperature as shown in Fig. 3(c). The heat film was a purchased commercial heating film made of PI film as substrate and copper coil as heating source. The size was 50 × 15 × 0.1 mm, and the film covered the SMPC surface completely avoiding the temperature distribution in the transverse direction. The loading profile was controlled by the power supply, the resistance of the heater was 25Ω, and the supplied DC power was 20 V. As the power was turned on, the temperature monitored by the thermal couple can reach 130 °C in 10s, and back to room temperature in 10s after power off. The parameters were selected to achieve the response time of 10s to demonstrate a swift reaction. The deformed gripper will unfreeze as heated, it tends to recover the initial shape, but the fixed detector constrains the recovery, and the reacting force can be recorded. The recovery force and temperature data will be recorded to describe the thermal-mechanical behavior. For the recovery angle measurement, the fixed force detector was removed, and the end can recover freely. The recovery angle is defined as the angle between the tangent lines of the free end and the fixed end, as shown in Fig. 3(d).

2.5. Functionality test

The grip tests were conducted to demonstrate the functionality and adaptability of the proposed compliant robotic grip structure. A grip test on a typical target was performed to show the working process. Then, compliance and working load test was conducted on various targets to prove the feasibility of the structure.

3. Results and discussion

3.1. Viscoelastic behavior

The glass transition temperature T_g of the sample is 132.53 °C based on the DMA results. Considering the thermal aging effect at temperatures above T_g is not preferred, the working temperature is limited below 130 °C. To describe and simulate the time-dependent mechanical behavior, the shape memory effect is modeled by the viscoelastic creep behavior in the formation of the Prony series as

$$E(t) = E_\infty + \sum_{i=1}^{N} E_i e^{-\frac{t}{\tau_i}} \quad (1)$$

where E(t) denotes the relaxation modulus, t is the absolute time during the creep test, E_∞ stands for the rubbery asymptotic modulus, E_i are the Prony series coefficients, and τ_i are the relaxation times. The DMA data were fitted with the Prony series as shown in Table 1.

The temperature-dependent behavior is described by the WLF equation as

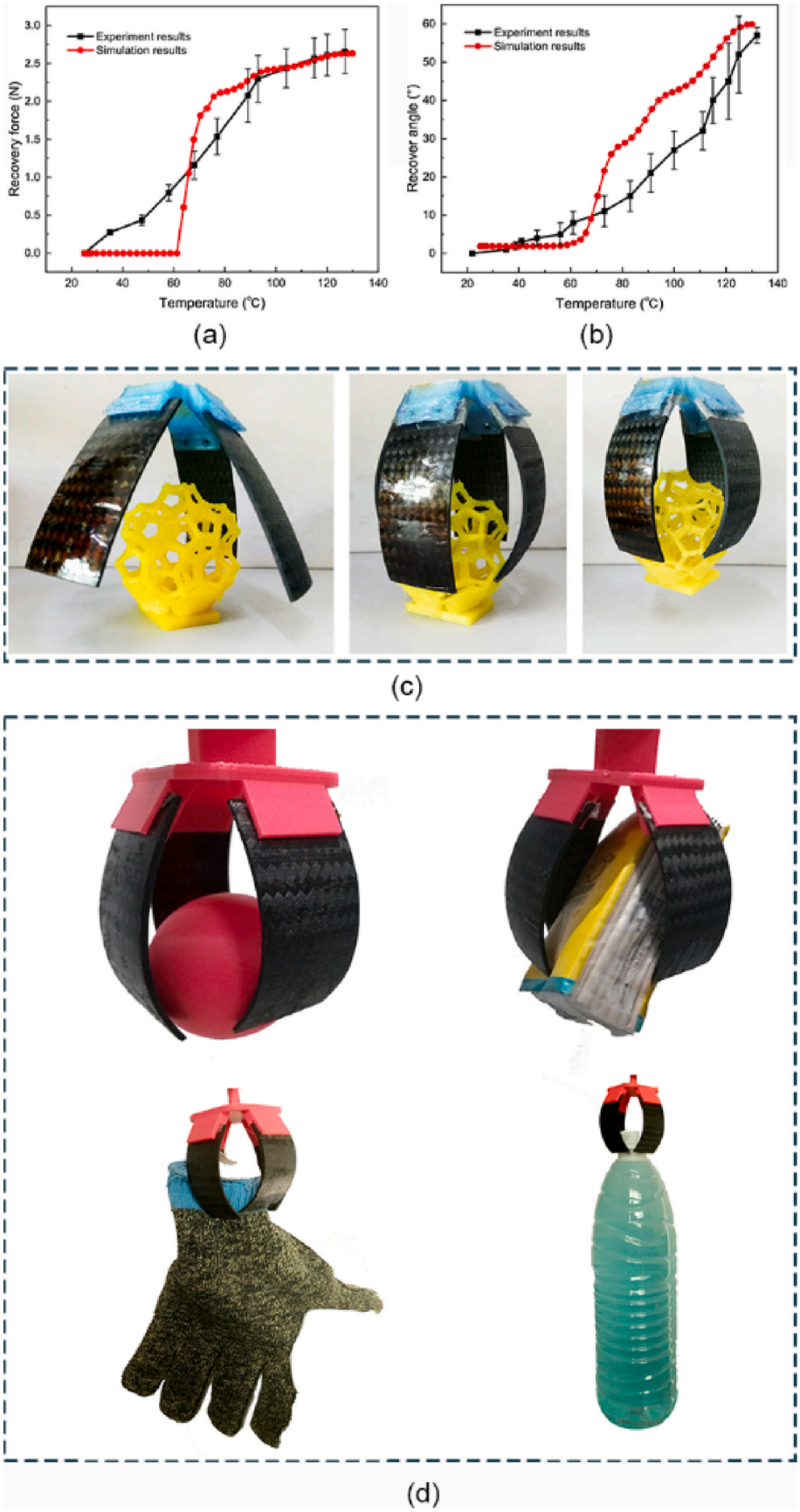

Fig. 5. Test of target grip performance. (a) Recovery force and (b) recovery angle of single gripper (c) Functionality test of target capture and movement. (d) Adaptability test.

$$\log(a_T) = \frac{-C_1(T - T_r)}{C_2 + (T - T_r)} \quad (2)$$

where a_T is the WLF shift factor, T is the temperature, T_r is the reference temperature selected to develop the compliance master curve, and C_1, and C_2 are constants fitted by DMA data. The WLF equation parameters of the SMPC are listed in Table 2.

3.2. Simulation of shape memory effect

The data of recovery force and recovery angle in the final phase obtained from the end-fixed model and end-free model is plotted in Fig. 4(a). As suggested by the data, no recovery is observed as the temperature is below 60 °C since the elastic strain in the polymer network is frozen by the crystallization of the transition phase. As the part is continuously heated, the polymer chains are free to move to recover the initial configuration. The recovery force and angle increase with a high rate at temperatures from 60 to 80 °C, then the varying slows down until the end. The maximum recovery force reaches 2.6 N, and the recovery angle of 60° indicates fully recovery demonstrating good shape memory capability. As shown in Fig. 4(b), in the initial deformation phase, the maximum strain and stress accumulate to 0.02314 and 4.26 MPa, respectively, as the external force is applied. In the following cooling phase from 10s to 30s, elastic strain decreases slightly since the creep rate is magnificently reduced at low temperature and von Mises stress is partially released to 0.95 MPa. In the final recovery phase, as the temperature increases, the stress and strain regain the initial status completing the shape memory process. The whole process reveals a typical cycle of the shape memory effect, and the model proves that the methodology is feasible for further study.

3.3. Performance test

The evaluation results of the recovery force and recovery angle with temperature are shown in Fig. 5(a) and (b). The test outcomes match well with the simulation results suggesting that the modeling method is correct and valuable for structure design and system evaluation. Variation exists at the beginning of the recovery phase, and this error is contributed by the model simplification and assumption on heating film entity neglection which overlooks the effect of thermal distribution inducing partially unfreezing of the polymer matrix further causes localized recovery at a low temperature value.

The functionality test is presented in Fig. 5(c). The predeformed grip structure was placed above the target, then the SMPC gripper was heated to 130 °C and recovered to the initial curving state gradually in 10s. After a cooling time of 10s, the whole structure was manually lifted 3 cm vertically while the target remained captured. During the process, the system completed the grasp and moved task compliantly and safely. The SMPC gripper is proved to be promising for capture work and movement tasks.

Further adaptability tests were conducted following the functionality test as shown in Fig. 5(d). Targets with various shapes, sizes, stiffness, and weight were compliantly captured following the previous steps. The results present the robustness and universality of the structure that the gripper can adapt to variations in object characters. Besides, the high elastic modulus of SMPCs by the enhancement phase provides impressive load capacity. The force cell was fixed against the SMPC part to record the reaction force at the free end, and the data precision is 0.1 N. the maximum load of the structure can reach 1.6 kg with the lifting ratio (object mass/gripper mass) reaching 106.6 which is magnificent among the gripping structures. Furthermore, even if the size of the object exceeds the range of the gripper, grippers with the proper size can be assembled to meet the requirement. Such a device with adaptability and universality has a promising future in applications in space, medicine, vehicles, etc.

4. Conclusion

A compliant robotic grip structure based on the SMPC without complex servo and execute units was demonstrated, and investigation results on the material property, structure performance, and system functionality were presented. The facility was designed and fabricated with a configuration of the finger-hand assembly. Then, the time- and temperature-dependent mechanical property of the SMPC sample was characterized by DMA and described by the Prony series and WLF equation, and results showed strong shape memory effect during thermal and mechanical loading-unloading cycles. The shape memory effect was investigated by mechanical response and energy conservation in the recovery force model and recovery angle model, and the results consistent with the experimental data indicating 100% recovery and grip force 2.6 N. Finally, the grip functionality and adaptivity were proved by target capture tests, and an impressive lifting ratio of 106 was illustrated indicating the potential for wide applications in the future. The broad implication of this research work is that a framework and methodology of numerical verification and experimental realization are developed for the functional structures based on SMPCs.

CRediT authorship contribution statement

Yonglin Zhang: Conceptualization, Methodology, Software, Investigation, Writing – original draft. **Tianzhen Liu:** Validation, Data curation, Investigation, Writing – review & editing. **Xin Lan:** Validation, Investigation. **Yanju Liu:** Supervision. **Jinsong Leng:** Supervision. **Liwu Liu:** Supervision, Writing – review & editing.

Declaration of competing interest

The authors declare that they have no known competing financial interests or personal relationships that could have appeared to influence the work reported in this paper.

Data availability

Data will be made available on request.

References

[1] J. Shintake, V. Cacucciolo, D. Floreano, H. Shea, Soft robotic grippers, Adv. Mater. 30 (2018), https://doi.org/10.1002/adma.201707035.
[2] T. George Thuruthel, Y. Ansari, E. Falotico, C. Laschi, Control strategies for soft robotic manipulators: a survey, Soft Robot. 5 (2018) 149–163, https://doi.org/10.1089/soro.2017.0007.
[3] N. El-Atab, R.B. Mishra, F. Al-Modaf, L. Joharji, A.A. Alsharif, H. Alamoudi, M. Diaz, N. Qaiser, M.M. Hussain, Soft actuators for soft robotic applications: a review, Adv. Intell. Syst. 2 (2020), 2000128, https://doi.org/10.1002/aisy.202000128.
[4] H.K. Yap, H.Y. Ng, C.H. Yeow, High-force soft printable pneumatics for soft robotic applications, Soft Robot. 3 (2016) 144–158, https://doi.org/10.1089/soro.2016.0030.
[5] M.A. Robertson, H. Sadeghi, J.M. Florez, J. Paik, Soft pneumatic actuator fascicles for high force and reliability, Soft Robot. 4 (2017) 23–32, https://doi.org/10.1089/soro.2016.0029.
[6] C.H. Liu, G.F. Huang, C.H. Chiu, T.Y. Pai, Topology synthesis and optimal design of an adaptive compliant gripper to maximize output displacement, J. Intell. Robot. Syst. Theory Appl. 90 (2018) 287–304, https://doi.org/10.1007/s10846-017-0671-x.
[7] L. Tian, J. Zheng, N.M. Thalmann, H. Li, Q. Wang, J. Tao, Y. Cai, Design of a single-material complex structure anthropomorphic robotic hand, Micromachines 12 (2021) 1–13, https://doi.org/10.3390/mi12091124.
[8] U. Deole, R. Lumia, M. Shahinpoor, M. Bermudez, Design and test of IPMC artificial muscle microgripper, J. Micro-Nano Mechatronics. 4 (2008) 95–102, https://doi.org/10.1007/s12213-008-0004-z.
[9] S. Taccola, F. Greco, E. Sinibaldi, A. Mondini, B. Mazzolai, V. Mattoli, Toward a new generation of electrically controllable hygromorphic soft actuators, Adv. Mater. 27 (2015) 1668–1675, https://doi.org/10.1002/adma.201404772.
[10] G.K. Lau, K.R. Heng, A.S. Ahmed, M. Shrestha, Dielectric elastomer fingers for versatile grasping and nimble pinching, Appl. Phys. Lett. 110 (2017), https://doi.org/10.1063/1.4983036.

[11] H. Il Kim, M.W. Han, S.H. Song, S.H. Ahn, Soft morphing hand driven by SMA tendon wire, Compos. B Eng. 105 (2016) 138–148, https://doi.org/10.1016/j.compositesb.2016.09.004.
[12] O.A. Araromi, S. Rosset, H.R. Shea, High-resolution, large-area fabrication of compliant electrodes via laser ablation for robust, stretchable dielectric elastomer actuators and sensors, ACS Appl. Mater. Interfaces 7 (2015) 18046–18053, https://doi.org/10.1021/acsami.5b04975.
[13] G. Kofod, W. Wirges, M. Paajanen, S. Bauer, Energy minimization for self-organized structure formation and actuation, Appl. Phys. Lett. 90 (2007) 1–4, https://doi.org/10.1063/1.2695785.
[14] G.J. Monkman, Advances in shape memory polymer actuation, Mechatronics 10 (2000) 489–498, https://doi.org/10.1016/S0957-4158(99)00068-9.
[15] L. Sun, W.M. Huang, Z. Ding, Y. Zhao, C.C. Wang, H. Purnawali, C. Tang, Stimulus-responsive shape memory materials: a review, Mater. Des. 33 (2012) 577–640, https://doi.org/10.1016/j.matdes.2011.04.065.
[16] J.M. Gallardo Fuentes, P. Gümpel, J. Strittmatter, Phase change behavior of nitinol shape memory alloys, Adv. Eng. Mater. 4 (2002) 437–452, https://doi.org/10.1002/1527-2648(20020717)4:7<437::AID-ADEM437>3.0.CO;2-8.
[17] N. Ma, G. Song, H.J. Lee, Position control of shape memory alloy actuators with internal electrical resistance feedback using neural networks, Smart Mater. Struct. 13 (2004) 777–783, https://doi.org/10.1088/0964-1726/13/4/015.
[18] C.C. Lan, C.H. Fan, An accurate self-sensing method for the control of shape memory alloy actuated flexures, Sensors Actuators, A Phys. 163 (2010) 323–332, https://doi.org/10.1016/j.sna.2010.07.018.
[19] J. Mohd Jani, M. Leary, A. Subic, M.A. Gibson, A review of shape memory alloy research, applications and opportunities, Mater. Des. 56 (2014) 1078–1113, https://doi.org/10.1016/j.matdes.2013.11.084.
[20] X. Zhang, P. Feng, Y. He, T. Yu, Q. Sun, Experimental study on rate dependence of macroscopic domain and stress hysteresis in NiTi shape memory alloy strips, Int. J. Mech. Sci. 52 (2010) 1660–1670, https://doi.org/10.1016/j.ijmecsci.2010.08.007.
[21] J. Leng, X. Lan, Y. Liu, S. Du, Shape-memory polymers and their composites: stimulus methods and applications, Prog. Mater. Sci. 56 (2011) 1077–1135, https://doi.org/10.1016/j.pmatsci.2011.03.001.
[22] Y. Liu, H. Du, L. Liu, J. Leng, Shape memory polymers and their composites in aerospace applications: a review, Smart Mater. Struct. 23 (2014), https://doi.org/10.1088/0964-1726/23/2/023001.
[23] J. Leng, H. Lu, Y. Liu, W.M. Huang, S. Du, Shape-memory polymers - a class of novel smart materials, MRS Bull. 34 (2009) 848–855, https://doi.org/10.1557/mrs2009.235.
[24] N. Besse, S. Rosset, J.J. Zarate, H. Shea, Flexible active skin: large reconfigurable arrays of individually addressed shape memory polymer actuators, Adv. Mater. Technol. 2 (2017) 1–8, https://doi.org/10.1002/admt.201700102.
[25] S. Yun, Z. Yu, X. Niu, W. Hu, L. Li, P. Brochu, Q. Pei, Compliant composite electrodes and large strain bistable actuation, Electroact. Polym. Actuators Devices 8340 (2012), 834012, https://doi.org/10.1117/12.915518, 2012.
[26] A. Rakow, K. Hedin, B. Anthony, Development of high specific power solar arrays with shape memory polymer hinge-lines, AIAA Spacecr. Struct. Conf. (2018) 1–11, https://doi.org/10.2514/6.2018-2206, 2018. 0.
[27] T. Liu, L. Liu, M. Yu, Q. Li, C. Zeng, X. Lan, Y. Liu, J. Leng, Integrative hinge based on shape memory polymer composites: material, design, properties and application, Compos. Struct. 206 (2018) 164–176, https://doi.org/10.1016/j.compstruct.2018.08.041.
[28] W. Wang, C.Y. Yu, P.A. Abrego Serrano, S.H. Ahn, Soft grasping mechanisms composed of shape memory polymer based self-bending units, Compos. B Eng. 164 (2019) 198–204, https://doi.org/10.1016/j.compositesb.2018.10.081.
[29] X. Lan, Y. Liu, H. Lv, X. Wang, J. Leng, S. Du, Fiber reinforced shape-memory polymer composite and its application in a deployable hinge, Smart Mater. Struct. 18 (2) (2009), 024002, https://doi.org/10.1088/0964-1726/18/2/024002.